

# Quasi-vacuum solar neutrino oscillations

G.L. Fogli<sup>a</sup>, E. Lisi<sup>a</sup>, D. Montanino<sup>b</sup>, and A. Palazzo<sup>a</sup>

<sup>a</sup> *Dipartimento di Fisica and Sezione INFN di Bari,*

*Via Amendola 173, I-70126 Bari, Italy*

<sup>b</sup> *Dipartimento di Scienza dei Materiali dell'Università di Lecce,*

*Via Arnesano, I-73100 Lecce, Italy*

## Abstract

We discuss in detail solar neutrino oscillations with  $\delta m^2/E$  in the range  $[10^{-10}, 10^{-7}]$  eV<sup>2</sup>/MeV. In this range, which interpolates smoothly between the so-called “just-so” and “Mikheyev-Smirnov-Wolfenstein” oscillation regimes, neutrino flavor transitions are increasingly affected by matter effects as  $\delta m^2/E$  increases. As a consequence, the usual vacuum approximation has to be improved through the matter-induced corrections, leading to a “quasi-vacuum” oscillation regime. We perform accurate numerical calculations of such corrections, using both the true solar density profile and its exponential approximation. Matter effects are shown to be somewhat overestimated in the latter case. We also discuss the role of Earth crossing and of energy smearing. Prescriptions are given to implement the leading corrections in the quasi-vacuum oscillation range. Finally, the results are applied to a global analysis of solar  $\nu$  data in a three-flavor framework.

PACS number(s): 26.65.+t, 14.60.Pq

## I. INTRODUCTION

A well-known explanation of the solar  $\nu_e$  flux deficit [1] is provided by flavor oscillations [2] of neutrinos along their way from the Sun ( $\odot$ ) to the Earth ( $\oplus$ ). For two active neutrino states [say,  $(\nu_e, \nu_\mu)$  in the flavor basis and  $(\nu_1, \nu_2)$  in the mass basis], the physics of solar  $\nu$  oscillations is governed, at any given energy  $E$ , by the mass-mixing parameters  $\delta m^2$  and  $\omega$  in vacuum,<sup>1</sup> as well as by the electron density profile  $N_e(x)$  in matter [3].

Different oscillation regimes can be identified in terms of three characteristics lengths, namely, the astronomical unit

$$L = 1.496 \times 10^8 \text{ km} , \quad (1)$$

the oscillation length in vacuum

$$L_{\text{osc}} = \frac{4\pi E}{\delta m^2} = 2.48 \times 10^{-3} \left( \frac{\delta m^2/E}{\text{eV}^2/\text{MeV}} \right)^{-1} \text{ km} , \quad (2)$$

and the refraction length in matter

$$L_{\text{mat}} = \frac{2\pi}{\sqrt{2}G_F N_e} = 1.62 \times 10^4 \left( \frac{N_e}{\text{mol}/\text{cm}^3} \right)^{-1} \text{ km} , \quad (3)$$

which is associated to the effective mixing angle  $\omega_m$  [3],

$$\sin^2 2\omega_m = \frac{\sin^2 2\omega}{(\cos 2\omega - L_{\text{osc}}/L_{\text{mat}})^2 + \sin^2 2\omega} . \quad (4)$$

Typical solutions to the solar neutrino problem (see, e.g., [4]) involve values of  $L_{\text{osc}}$  either in the so-called “just-so” (JS) oscillation regime [5], characterized by

$$L_{\text{osc}}^{\text{JS}} \sim L \gg L_{\text{mat}} , \quad (5)$$

or in the “Mykheyev-Smirnov-Wolfenstein” (MSW) oscillation regime [3], characterized by

$$L_{\text{osc}}^{\text{MSW}} \sim L_{\text{mat}} \ll L . \quad (6)$$

The two regimes correspond roughly to  $\delta m^2/E \sim O(10^{-11}) \text{ eV}^2/\text{MeV}$  and to  $\delta m^2/E \gtrsim 10^{-7} \text{ eV}^2/\text{MeV}$ , respectively.

For just-so oscillations, since  $L_{\text{mat}}/L_{\text{osc}} \rightarrow 0$ , the effect of matter is basically to suppress the oscillation amplitude both in the Sun and in the Earth ( $\sin^2 2\omega_m \rightarrow 0$ ), so that (coherent) flavor oscillations take place only in vacuum, starting from the Sun surface [6]. Conversely, for MSW oscillations,  $L_{\text{osc}} \sim L_{\text{mat}}$  and flavor transitions are dominated by the detailed matter density profile, while the many oscillation cycles in vacuum ( $L_{\text{osc}} \ll L$ ) are responsible for complete  $\nu$  decoherence at the Earth, once smearing effects are taken into account [7].

---

<sup>1</sup>One can take  $\delta m^2 = m_2^2 - m_1^2 > 0$ , as far as  $\omega$  is taken in the first quadrant  $[0, \frac{\pi}{2}]$ .

Therefore, it is intuitively clear that in the intermediate range between (5) and (6), corresponding approximately to  $10^{-10} \lesssim \delta m^2/E \lesssim 10^{-7}$  eV<sup>2</sup>/MeV, the simple vacuum oscillation picture of the JS regime becomes increasingly decoherent and affected by matter effects for increasing values of  $\delta m^2/E$ , leading to a hybrid regime that might be called of “quasi-vacuum” (QV) oscillations, characterized by

$$L_{\text{mat}} \lesssim L_{\text{osc}}^{\text{QV}} \lesssim L, \quad (7)$$

In the past, quasi-vacuum effects on the oscillation amplitude and phase have been explicitly considered only in relatively few papers (see, e.g., [8–14]) as compared with the vast literature on solar neutrino oscillations, essentially because typical fits to solar  $\nu$  rates allowed only marginal solutions in the range where QV effects are relevant. However, more recent analyses appear to extend the former ranges of the JS solutions *upwards* [15] and of the MSW solutions *downwards* [16] in  $\delta m^2/E$ , making them eventually merge in the QV range [17], especially under generous assumptions about the experimental or theoretical  $\nu$  flux uncertainties.<sup>2</sup> Therefore, a fresh look at QV corrections seems warranted. In particular, quasi-vacuum effects have been recently revisited in [18,19], where a semianalytical approximation was discussed to correct the familiar just-so formula in the QV regime. In this work we go beyond approximate results, and discuss their limitations, by performing accurate numerical calculations which include the exact density profile in the Sun and in the Earth, within the reference mass-mixing ranges  $\delta m^2/E \in [10^{-10}, 10^{-7}]$  eV<sup>2</sup>/MeV and  $\tan^2 \omega \in [10^{-3}, 10]$ .<sup>3</sup> We then apply such calculations to a global analysis of solar neutrino data in the range  $\delta m^2 \leq 10^{-8}$  eV<sup>2</sup>.

Our paper is structured as follows. The basic notation and the numerical techniques used in the calculations are introduced in Sec. II and III, respectively. The effects of solar matter in the quasi-vacuum oscillation regime are discussed in Sec. IV, where the results for true and exponential density profiles are compared. Earth matter effects are described in Sec. V. The decoherence of oscillations induced by energy (and time) integration is discussed in Sec. VI. The basic results are summarized and organized in Sec. VII, and then applied to a three-flavor oscillation analysis in Sec. VIII. Section IX concludes our work.

## II. NOTATION

The  $\nu$  propagation from the Sun core to the detector at the Earth can be interpreted as a “double slit experiment,” where the original  $\nu_e$  can take two paths, corresponding to the intermediate transitions  $\nu_e \rightarrow \nu_1$  and to  $\nu_e \rightarrow \nu_2$ . The global  $\nu_e$  survival amplitude is then the sum of the amplitudes along the two paths,

---

<sup>2</sup>Such extended range for current solutions reflects, in part, the lack of a strong, model-independent signature of energy dependence in the solar neutrino deficit.

<sup>3</sup> The variable  $\tan^2 \omega$  is useful to chart the first two octants of the mixing angle range [16,20].

$$\begin{aligned}
A(\nu_e \rightarrow \nu_e) &= A_{\odot}(\nu_e \rightarrow \nu_1) \cdot A_{\text{vac}}(\nu_1 \rightarrow \nu_1) \cdot A_{\oplus}(\nu_1 \rightarrow \nu_e) \\
&+ A_{\odot}(\nu_e \rightarrow \nu_2) \cdot A_{\text{vac}}(\nu_2 \rightarrow \nu_2) \cdot A_{\oplus}(\nu_2 \rightarrow \nu_e) ,
\end{aligned} \tag{8}$$

where the transition amplitudes from the Sun production point to its surface ( $A_{\odot}$ ), from the Sun surface to the Earth surface ( $A_{\text{vac}}$ ) and from the Earth surface to the detector ( $A_{\oplus}$ ) have been explicitly factorized. The  $\nu_e$  survival probability  $P_{ee}$  is then given by

$$P_{ee} = |A(\nu_e \rightarrow \nu_e)|^2 . \tag{9}$$

In general, the above amplitudes can be written as

$$A_{\odot}(\nu_e \rightarrow \nu_1) = \sqrt{P_{\odot}} \exp(i\xi_{\odot}) , \tag{10a}$$

$$A_{\text{vac}}(\nu_1 \rightarrow \nu_1) = \exp\left(-i m_1^2 (L - R_{\odot})/2E\right) , \tag{10b}$$

$$A_{\oplus}(\nu_1 \rightarrow \nu_e) = \sqrt{P_{\oplus}} \exp(i\xi_{\oplus}) , \tag{10c}$$

for the first path and as

$$A_{\odot}(\nu_e \rightarrow \nu_2) = \sqrt{1 - P_{\odot}} , \tag{11a}$$

$$A_{\text{vac}}(\nu_2 \rightarrow \nu_2) = \exp\left(-i m_2^2 (L - R_{\odot})/2E\right) , \tag{11b}$$

$$A_{\oplus}(\nu_2 \rightarrow \nu_e) = \sqrt{1 - P_{\oplus}} , \tag{11c}$$

for the second path, where  $R_{\odot}$  is the Sun radius.<sup>4</sup> In the above equations,  $P_{\odot}$  and  $P_{\oplus}$  are real numbers ( $\in [0, 1]$ ) representing the transition probability  $P(\nu_e \leftrightarrow \nu_1)$  along the two partial paths inside the Sun (up to its surface) and inside the Earth (up to the detector). The corresponding phase differences between the two paths,  $\xi_{\odot}$  and  $\xi_{\oplus}$  ( $\in [0, 2\pi]$ ), have been associated to the first path without loss of generality. The  $\nu_e$  survival probability  $P_{ee}$  from Eq. (9) reads then

$$\begin{aligned}
P_{ee} &= P_{\odot}P_{\oplus} + (1 - P_{\odot})(1 - P_{\oplus}) \\
&+ 2\sqrt{P_{\odot}(1 - P_{\odot})P_{\oplus}(1 - P_{\oplus})} \cos \xi ,
\end{aligned} \tag{12}$$

where the global oscillation phase is given by

$$\xi = \frac{\delta m^2 L}{2E} (1 - \delta_R - \delta_{\odot} - \delta_{\oplus}) , \tag{13}$$

with the definitions

$$\delta_R = \frac{R_{\odot}}{L} = 4.7 \times 10^{-3} , \tag{14}$$

$$\delta_{\odot} = \frac{2E}{\delta m^2 L} \xi_{\odot} , \tag{15}$$

$$\delta_{\oplus} = \frac{2E}{\delta m^2 L} \xi_{\oplus} . \tag{16}$$

---

<sup>4</sup>Although  $R_{\odot}$  is relatively small ( $R_{\odot}/L = 4.7 \times 10^{-3}$ ), it is explicitly kept for later purposes. The Earth radius  $R_{\oplus}$  can instead be safely neglected ( $R_{\oplus}/L = 4.3 \times 10^{-5}$ ).

A relevant extension of the  $2\nu$  formula (12) is obtained for  $3\nu$  oscillations, required to accommodate solar and atmospheric neutrino data [21]. Assuming a third mass eigenstate  $\nu_3$  with  $m^2 = |m_3^2 - m_{1,2}^2| \gg \delta m^2$ , the  $3\nu$  survival probability can be written as

$$P_{ee}^{3\nu} = c_\phi^4 P_{ee}^{2\nu} + s_\phi^4, \quad (17)$$

where  $\phi$  is the  $(\nu_e, \nu_3)$  mixing angle, and  $P_{ee}^{2\nu}$  is given by Eq. (12), *provided that* the electron density  $N_e$  is replaced everywhere by  $c_\phi^2 N_e$  (see [20] and refs. therein). Such replacement implies that the  $3\nu$  case is not a simple mapping of the  $2\nu$  case, and requires specific calculations for any given value of  $\phi$ .

We conclude this section by recovering more familiar expressions for  $P_{ee}$ , as special cases of Eq. (12). The JS limit ( $L_{\text{mat}}/L_{\text{osc}} \rightarrow 0$ , with complete suppression of oscillations inside matter) corresponds to  $P_\odot \simeq c_\omega^2 \simeq P_\oplus$  and to negligible  $\delta_\odot, \delta_\oplus$ . Then, neglecting also  $\delta_R$ , one gets from (12) the standard “vacuum oscillation formula,”

$$P_{ee}^{\text{JS}} \simeq 1 - \sin^2 2\omega \sin^2(\pi L/L_{\text{osc}}). \quad (18)$$

In the MSW limit ( $L/L_{\text{osc}} \rightarrow \infty$ ), the global oscillation phase  $\xi$  is very large and  $\cos \xi \simeq 0$  on average. Furthermore, assuming for  $P_\odot$  a well-known approximation in terms of the “crossing” probability  $P_c$  between mass eigenstates in matter [in our notation,  $P_\odot \simeq \sin^2 \omega_m^0 P_c + \cos^2 \omega_m^0 (1 - P_c)$ , with  $\omega_m^0$  calculated at the production point], one gets from (12) the so-called Parke’s formula [22]

$$P_{ee}^{\text{MSW}} \simeq \frac{1}{2} + \left(\frac{1}{2} - P_c\right) \cos 2\omega \cos 2\omega_m^0, \quad (19)$$

where Earth matter effects have been neglected ( $P_\oplus \simeq c_\omega^2$ ).

### III. NUMERICAL TECHNIQUES

In general, numerical calculations of the  $\nu$  transition amplitudes must take into account the detailed  $N_e$  profile along the neutrino trajectory, both in the Sun and in the Earth.

Concerning the Sun, we take  $N_e$  from [23] (“year 2000” standard solar model). Figure 1 shows such  $N_e$  profile as a function of the normalized radius  $r/R_\odot$ , together with its exponential approximation [1]  $N_e = N_e^0 \exp(-r/r_0)$ , with  $N_e^0 = 245 \text{ mol/cm}^3$  and  $r_0 = R_\odot/10.54$ . For the exponential density profile, the neutrino evolution equations can be solved analytically [8–11]. In order to calculate the relevant probability  $P_\odot$  and the phase  $\xi_\odot$ , we have developed several computer programs which evolve numerically the familiar MSW neutrino evolution equations [3] along the Sun radius, for generic production points, and for any given value of  $\delta m^2/E \in [10^{-10}, 10^{-7}] \text{ eV}^2/\text{MeV}$  and of  $\tan^2 \omega$ . We estimate a numerical (fractional) accuracy of our results better than  $10^{-4}$ , as derived by several independent checks. As a first test, we integrate numerically the MSW equations both in their usual complex form (2 real + 2 imaginary components) and in their Bloch form involving three real amplitudes [24], obtaining the same results. We have then repeated the calculations with different integration routines taken from several computer libraries, and found no significant differences among the outputs. We have optionally considered, besides the exact  $N_e$  profile, also the

exponential profile, which allows a further comparison of the numerical integration of the MSW equations with their analytical solutions, as worked out in [10,11] in terms of hypergeometric functions (that we have implemented in an independent code). Also in this case, no difference is found between the output of the different codes.

Concerning the calculation of the quantities  $P_{\oplus}$  and  $\xi_{\oplus}$  in the Earth, we evolve analytically the MSW equations at any given nadir angle  $\eta$ , using the technique described in [25], which is based on a five-step biquadratic approximation of the density profile from the Preliminary Reference Earth Model (PREM) [26] and on a first-order perturbative expansion of the neutrino evolution operator. Such analytical technique provides results very close to a full numerical evolution of the neutrino amplitudes, the differences ( $\lesssim 10^{-3}$ ) being smaller than those induced by uncertainties in  $N_e$  [25], as we have checked in the whole mass-mixing range considered in this work. In conclusion, we are confident in the accuracy of our results, which are discussed in the following sections.

#### IV. MATTER EFFECTS IN THE SUN

Figure 2 shows, in the mass-mixing plane and for standard solar model density, isolines of the difference  $c_{\omega}^2 - P_{\odot}$  (solid curves), which becomes zero in the just-so oscillation limit of very small  $\delta m^2/E$ . The isolines shape reminds the “lower corner” of the more familiar MSW triangle [22]. Also shown are isolines of constant resonance radius  $R_{\text{res}}/R_{\odot}$  (dotted curves), defined by the MSW resonance condition  $L_{\text{osc}}/L_{\text{mat}}(R_{\text{res}}) = \cos 2\omega$ . The values of  $c_{\omega}^2 - P_{\odot}$  are already sizable (a few percent) at  $\delta m^2/E \sim 10^{-9}$ , and increase for increasing  $\delta m^2/E$  and for large mixing [ $\tan^2 \omega \sim O(1)$ ], especially in the first octant, where the MSW resonance can occur. The difference between matter effects in the first and in the second octant can lead to observable modifications of the allowed regions in fits to the data [19], and to a possible discrimination between the cases  $\omega < \frac{\pi}{4}$  and  $\omega > \frac{\pi}{4}$  [17,19].

In the whole parameter range of Fig. 2, it turns out that, within the region of  $\nu$  production ( $r/R_{\odot} \lesssim 0.3$ ), it is  $L_{\text{mat}}(r) \ll L_{\text{osc}}$  (and thus  $\sin^2 2\omega_m^0 \simeq 0$ ).<sup>5</sup> As a consequence, all the curves of Fig. 2 do not depend on the specific  $\nu$  production point (as we have also checked numerically), and no smearing over the  $\nu$  source distribution is needed in the quasi-vacuum regime. This is a considerable simplification with respect to the MSW regime, which involves higher values of  $\delta m^2/E$  and thus shorter (resonance) radii, which are sensitive to the detailed  $\nu$  source distribution.

Figure 3 shows, in the same coordinates of Fig. 2, the isolines of  $c_{\omega}^2 - P_{\odot}$  corresponding to the exponential density profile (dotted curves), for which we have used the fully analytical results of [10,11]. (Identical results are obtained by numerical integration.) The solid lines in Fig. 3 refer to a well-known approximation (sometimes called “semianalytical”) to such results, which is obtained in the limit  $N_e \rightarrow 0$  at the Sun surface (it is not exactly so for the exponential profile, see Fig. 1). More precisely, the zeroth order expansion of the hypergeometric functions [10,11] in terms of the small parameter  $z_0 = i\sqrt{2}G_F r_0 N_e(R_{\odot})$  ( $|z_0| \simeq 0.16$ ) gives, for  $N_e(0) \rightarrow \infty$ , the result  $P_{\odot} \simeq [\exp(\gamma c_{\omega}^2) - 1]/[\exp(\gamma) - 1]$  with  $\gamma = \pi r_0 \Delta m^2/E$  [10],

---

<sup>5</sup>This is also indicated by the fact that  $R_{\text{res}}/R_{\odot} \gtrsim 0.55$  in the  $\delta m^2/E$  range of Fig. 2.

which leads to the QV prescription discussed in [19]. The differences between the solid and dotted curves in Fig. 3 are essentially due to the “solar border approximation” ( $N_e \rightarrow 0$ ) assumed in the semianalytical case; indeed, the differences would practically vanish if the exponential density profile, and thus the “effective” Sun radius, were unphysically continued for  $r \gg R_\odot$  (not shown). Such limitations of the semianalytical approximation have been qualitatively suggested by the authors of [27] but, contrary to their claim, our Fig. 3 shows explicitly that the semianalytical calculation of  $P_\odot$  represents a reasonable approximation to the analytical one for  $\omega$  in *both* octants, as also verified in [28].

A comparison of the results of Fig. 2 (true density) and of Fig. 3 (exponential density) shows that, in the latter case, the correction term  $c_\omega^2 - P_\odot$  tends to be somewhat over-estimated, in particular when the semianalytical approximation is used. We have verified that such bias is dominantly due to the difference (up to a factor of  $\sim 2$ ) between the true density profile and its exponential approximation around  $r/R_\odot \sim 0.8$  (see Fig. 1) and, subdominantly, to the details of the density profile shape at the border ( $r/R_\odot \rightarrow 1$ ). As a consequence, the “exponential profile” calculation of  $P_\odot$  (either semianalytic [17,19] or analytic) tends to shift systematically the onset of solar matter effects to lower values of  $\delta m^2/E$ . For instance, at  $\tan^2 \omega \simeq 1$  (maximal mixing), the value  $c_\omega^2 - P_\odot = 0.05$  is reached at  $\delta m^2/E \simeq 8 \times 10^{-10}$  eV<sup>2</sup>/MeV for the true density, and at  $\delta m^2/E$  a factor of  $\sim 2$  lower for the exponential density. In order to avoid artificially larger effects at low  $\delta m^2/E$  in neutrino data analyses, one should calculate  $P_\odot$  with the true electron density profile.

Concerning the phase factor  $\delta_\odot$ , we confirm earlier indications [12,13] about its smallness, in both cases of true and exponential density. In the latter case, the semianalytic approximation gives [11,12], for  $\delta m^2/E \rightarrow 0$ , the  $\omega$ -independent result

$$\delta_\odot \simeq L^{-1} \left\{ r_0 \left[ \ln(\sqrt{2} G_F N_e^0 r_0) + \gamma_E \right] - R_\odot \right\} , \quad (20)$$

where  $\gamma_E (\simeq 0.577)$  is the Euler constant. Numerically,  $\delta_\odot^0 \simeq -5.39 \times 10^{-4}$ , much smaller than  $\delta_R$ . As far as  $\delta m^2/E \lesssim 10^{-8}$  ( $10^{-7}$ ) eV<sup>2</sup>/MeV, we find that  $\delta_\odot$  differs from such value by less than 20% (50%), the exact difference depending on the value of  $\tan^2 \omega$  (not shown). Therefore,  $\delta_\odot$  is an order of magnitude smaller than  $\delta_R$  in the whole mass-mixing range considered. A similar behavior is found by using the true density profile ( $\delta_\odot \lesssim 10^{-3}$  everywhere). As for  $P_\odot$ , we find also for  $\delta_\odot$  no significant dependence on the neutrino production point in the Sun core.

In conclusion, we find only modest differences between the analytical calculations of  $P_\odot$ , based on the exponential density profile, and its semianalytical approximation. The difference with respect to the numerical calculation of  $P_\odot$ , based on the standard solar model profile, is instead more pronounced, and leads to a factor of  $\sim 2$  difference in the value of  $\delta m^2/E$  where QV effects start to be significant. Therefore, we recommend the use of the electron profile from the standard solar model, implying numerical calculations of  $P_\odot$ .<sup>6</sup> Concerning the phase  $\delta_\odot$ , it simply shifts the global oscillation phase  $\xi$  in Eq. (12) by less than one permill, and thus it can be safely neglected in all current applications.

---

<sup>6</sup>The interested reader can obtain numerical tables of  $P_\odot$ , calculated for the standard solar model density, upon request from the authors.

## V. MATTER EFFECTS IN THE EARTH

Strong Earth matter effects typically emerge in the range where  $L_{\text{osc}} \sim L_{\text{mat}}$  within the mantle ( $N_e \sim 2 \text{ mol/cm}^3$ ) or the core ( $N_e \sim 5 \text{ mol/cm}^3$ ), as well as in other ranges of mantle-core oscillation interference [29], globally corresponding to  $\delta m^2/E \sim 10^{-7}-10^{-6} \text{ eV}^2/\text{MeV}$ . Therefore, only marginal effects are expected in the parameter range considered in this work, as confirmed by the results reported in Fig. 4.

Figure 4 shows isolines of the quantity  $c_\omega^2 - P_\oplus$ , which becomes zero in the just-so oscillation limit of very small  $\delta m^2/E$ . The solid curves corresponds to a nadir angle  $\eta = 0^\circ$  (diametral crossing of neutrinos) and the dotted curves to  $\eta = 45^\circ$  (crossing of mantle only). For other values of  $\eta$  (not shown), the quantity  $c_\omega^2 - P_\oplus$  has a comparable magnitude. In the current neutrino jargon, the Earth effect shown in Fig. 4 is operative in the lowermost part of the so-called ‘‘LOW’’ MSW solution [16] to the solar neutrino problem, or, from another point of view, to the uppermost part of the vacuum solutions [15]. Concerning the phase correction  $\delta_\oplus$  (not shown), it is found to be smaller than  $1.5 \times 10^{-5}$  in the whole mass-mixing plane considered, and thus can be safely neglected.

In practical applications, the correction term  $c_\omega^2 - P_\oplus$  must be time-averaged. This poses, in principle, a tedious integration problem, since such correction appears, in Eq. (12), both in the amplitude of the oscillating term ( $\propto \cos \xi$ ) and in the remaining, non-oscillating term. While the integration over time can be transformed, for the non-oscillating term, into a more manageable integration over  $\eta$  [25], this cannot be done for the oscillating term, which depends on time both through the prefactor  $\sqrt{P_\oplus(1 - P_\oplus)}$  and through the phase  $\xi$  (via eccentricity effects). However, in region of the mass-mixing plane where the Earth effect is non-negligible (namely, where  $c_\omega^2 - P_\oplus \gtrsim \text{few } \%$ ), it turns out that  $P_\odot \sim 0$ , so that the total amplitude of the oscillating term is small. Moreover, as it will be discussed in the next section, energy smearing effects strongly suppress the oscillation factor  $\cos \xi$  in the same region. Therefore, for  $\delta m^2/E \gtrsim 10^{-8}$ , the oscillating term in Eq. (12) is doubly suppressed, and one can safely consider only the non-oscillatory terms.

## VI. DAMPING OF THE INTERFERENCE TERM

In the just-so regime, the interference factor  $\cos \xi$  in Eq. (12) can lead to an observable modulation both in the energy and in the time distribution of solar neutrino events. This modulation gradually disappears as  $\delta m^2/E$  increases, as a consequence of several decoherence effects ( $\langle \cos \xi \rangle \rightarrow 0$ ) [7,18], which are typically dominated by energy smearing [30]. The broader the neutrino spectrum, the lower the values of  $\delta m^2/E$  where decoherence becomes important: therefore, it suffices to consider the narrowest spectra (the so-called Be neutrino ‘‘lines’’ [31]) for illustration purposes.

Let us consider a  $\nu$  ‘‘line’’ energy spectrum  $s(E)$ , with  $\int dE s(E) = 1$  and  $\langle E \rangle = \int dE s(E) E$ . The energy-averaged oscillating factor,

$$C = \left\langle \cos \left( \frac{\delta m^2 L}{2E} \right) \right\rangle_E = \int dE s(E) \cos \left( \frac{\delta m^2 L}{2E} \right), \quad (21)$$

can be written, in the narrow-width approximation ( $\Delta E = E - \langle E \rangle \ll \langle E \rangle$ ), in terms of the Fourier transform of the spectrum,

$$\tilde{s}(\tau) = \int dE s(E) e^{i\Delta E \tau} . \quad (22)$$

More precisely,

$$C \simeq \int dE s(E) \cos \left( \frac{\delta m^2 L}{2\langle E \rangle} \left( 1 - \frac{\Delta E}{\langle E \rangle} \right) \right) \quad (23)$$

$$= D \cos \left( \frac{\delta m^2 L}{2\langle E \rangle} (1 - \delta) \right) , \quad (24)$$

where  $D = |\tilde{s}(\tau)|$ ,  $\delta = \tau^{-1} \langle E \rangle^{-1} \arg \tilde{s}(\tau)$ , and  $\tau = \delta m^2 L / 2\langle E \rangle^2$ .

Using the  $s(E)$  profile for the Be lines from [31], we find that the phase correction  $\delta$  is smaller than a few permill in the region where the damping factor  $D$  is greater than a few percent. If  $\delta$  is neglected, the average oscillation factor can be simply written as the oscillation factor at the average energy, times a damping term  $D$ :

$$\left\langle \cos \left( \frac{\delta m^2 L}{2E} \right) \right\rangle_E \simeq D \cdot \cos \left( \frac{\delta m^2 L}{2\langle E \rangle} \right) . \quad (25)$$

A similar approach to smearing effects for neutrino lines was developed in [13].

Figure 5 shows the damping factor  $D$  for the two Be neutrino lines at  $\langle E \rangle = 0.863$  and 0.386 MeV. The factor is negligible for  $\delta m^2 / E \gtrsim 10^{-8}$  eV<sup>2</sup>/MeV, implying that the oscillation pattern is completely smeared out in such range.<sup>7</sup> The onset of smearing effects is shifted to even lower values of  $\delta m^2 / E$  for continuous energy spectra. In conclusion, the integration over neutrino energy makes the average oscillation factor  $\langle \cos \xi \rangle$  always negligible in the range where Earth matter effects are important.

Finally, we recall that integration over time also acts as a damping factor. At first order in the eccentricity  $\epsilon$ , one has that  $L(t) \simeq L[1 - \epsilon \cos \alpha(t)]$  and  $\dot{\alpha}(t) \simeq 1 + 2\epsilon \cos \alpha$ , where  $\alpha$  is the orbital phase, and  $t \in [0, 2\pi]$  is the normalized time variable ( $t = 0$  at perihelion). Then the yearly average of  $\cos \xi$  [times the square-law factor  $L^2 / L^2(t)$ ] can be performed analytically [32], giving

$$\frac{1}{2\pi} \int_0^{2\pi} dt \frac{L^2}{L^2(t)} \cos \left( \frac{\delta m^2 L(t)}{2E} \right) \simeq J_0 \left( \epsilon \frac{\delta m^2 L}{2E} \right) \cos \left( \frac{\delta m^2 L}{2E} \right) , \quad (26)$$

where  $J_0$  is the Bessel function, acting as a further damping term for large values of its argument.<sup>8</sup>

---

<sup>7</sup>This range corresponds approximately to  $L_{\text{osc}} / L \lesssim w / \langle E \rangle$ , where  $w \sim O(1 \text{ keV})$  is the line width.

<sup>8</sup>We consider only yearly-averaged neutrino rates in this work. Seasonal variation effects will be studied elsewhere.

## VII. PRACTICAL RECIPES

We have seen in the previous sections that, as  $\delta m^2/E$  increases, the deviations of  $P_\odot$  (and subsequently of  $P_\oplus$ ) from the vacuum value  $c_\omega^2$  become increasingly important. We have also seen that the phase corrections  $\delta_\odot$  and  $\delta_\oplus$  are smaller than  $\delta_R = R_\odot/L$ , which can in turn be neglected in present applications,<sup>9</sup> so that one can practically take the usual vacuum value for the oscillation phase,  $\xi \simeq \delta m^2 L/2E$ . We think it useful to organize known and less known results through the following approximate expressions for the calculation of  $P_{ee}$ , which are accurate to better than 3% with respect to the exact, general formula (12) valid at any  $\delta m^2/E$ .

For  $\delta m^2/E \lesssim 5 \times 10^{-10}$  eV<sup>2</sup>/MeV, one can take  $P_\odot \simeq P_\oplus \simeq c_\omega^2$ , and obtain the just-so oscillation formula

$$P_{ee}^{\text{JS}} \simeq c_\omega^4 + s_\omega^4 + 2s_\omega^2 c_\omega^2 \cos \xi , \quad (27)$$

with  $\xi = \delta m^2 L/2E$ . For  $5 \times 10^{-10} \lesssim \delta m^2/E \lesssim 10^{-8}$  eV<sup>2</sup>/MeV, one can still take  $P_\oplus \simeq c_\omega^2$ , but since  $P_\odot \neq c_\omega^2$  (quasi-vacuum regime) one has that

$$P_{ee}^{\text{QV}} \simeq c_\omega^2 P_\odot + s_\omega^2 (1 - P_\odot) + 2s_\omega c_\omega \sqrt{P_\odot (1 - P_\odot)} \cos \xi , \quad (28)$$

where  $\xi = \delta m^2 L/2E$ , and  $P_\odot$  has to be calculated numerically.<sup>10</sup> Finally, for  $\delta m^2/E \gtrsim 10^{-8}$  eV<sup>2</sup>/MeV, also Earth matter effects are important ( $P_\oplus \neq c_\omega^2$ ); however, this complication is balanced by the disappearance of the oscillating term ( $\cos \xi \simeq 0$ ) due to unavoidable smearing effects, so that the usual MSW regime is recovered:

$$P_{ee}^{\text{MSW}} \simeq P_\oplus P_\odot + (1 - P_\oplus)(1 - P_\odot) . \quad (29)$$

Time averages are then relatively simple to implement. In Eqs. (27) and (28), the yearly averages of  $\cos \xi$  can be performed analytically [Eq. (26)]. In Eq. (29), the nighttime average of  $P_\oplus$  can be transformed into a more manageable integration over the nadir angle, both for yearly [25] and for seasonal [33] averages.

To summarize, the above sequence of equations describes the passage from the regime of just-so to that of MSW oscillations, via quasi-vacuum oscillations. In the JS regime, oscillations are basically coherent and do not depend on the electron density in the Earth or in the Sun ( $N_e \rightarrow \infty$ ). In the MSW regime, oscillations are basically incoherent ( $L \rightarrow \infty$ ) and, in general, depend on the detailed electron density profile of both the Sun and the Earth. In particular, in the MSW regime one has to take into account the interplay between the density profile and the neutrino source distribution profile. The intermediate QV regime is instead characterized by partially coherent oscillations (with increasing decoherence as

<sup>9</sup>Notice that  $R_\odot$  is an order of magnitude smaller than the eccentricity variation of the orbital radius:  $R_\odot/(L_{\text{max}} - L_{\text{min}}) = R_\odot/2\epsilon L = 0.14$ .

<sup>10</sup>As discussed in Sec. IV, the semianalytical approximation described in [19] for  $P_\odot^{\text{QV}}$ , although handy, tends to overestimate quasi-vacuum effects.

$\delta m^2/E$  increases), and by a sensitivity to the electron density of the Sun (but not of the Earth). Such sensitivity is not as strong as in the MSW regime and, in particular, QV effects are independent from the specific  $\nu$  production point, which can be effectively taken at the Sun center.

For the sake of completeness, we mention that, for high values of  $\delta m^2/E$  ( $\gg 10^{-4}$  eV<sup>2</sup>/), corresponding to  $L_{\text{osc}} \ll L_{\text{mat}}$  in the Sun, the sensitivity to matter effects is eventually lost both in the Sun and in the Earth ( $P_{\odot} \simeq P_{\oplus} \simeq c_{\omega}^2$ ), and one reaches a fourth regime sometimes called of energy-averaged (EA) oscillations, which is totally incoherent and  $N_e$ -independent:

$$P_{ee}^{\text{EA}} \simeq c_{\omega}^4 + s_{\omega}^4 . \quad (30)$$

Such regime, which predicts an energy-independent suppression of the solar neutrino flux, seems to be disfavored (but perhaps not yet ruled out) by current experimental data on total neutrino rates. In conclusion, for  $\delta m^2/E$  going from extremely low values to infinity, one can identify four rather different oscillation regimes,

$$\text{JS} \rightarrow \text{QV} \rightarrow \text{MSW} \rightarrow \text{EA} , \quad (31)$$

each being characterized by specific properties and applicable approximations. Experiments still have to tell us unambiguously which of them truly applies to solar neutrinos.

### VIII. THREE-FLAVOR OSCILLATION ANALYSIS

As discussed in [19], in the QV regime the  $2\nu$  survival probability (28) is non-symmetric with respect to the operation  $\omega \rightarrow \frac{\pi}{2} - \omega$ , which instead holds for JS oscillations [Eq. (27)].<sup>11</sup> Here we extend such observation to  $3\nu$  oscillations, under the hypothesis  $\delta m^2 \ll m^2$  which leads to Eq. (17). The  $2\nu$  case is recovered for  $\phi = 0$ .

Equation (17) for  $P_{3\nu}$  preserves the (a)symmetry properties of  $P_{2\nu}$  under the replacement  $\omega \rightarrow \frac{\pi}{2} - \omega$ . Therefore, while  $P_{3\nu}^{\text{JS}}$  [obtained from Eqs. (17) and (27)] is symmetric with respect to the  $\omega = \frac{\pi}{4}$  value, the expression of  $P_{3\nu}^{\text{QV}}$  [obtained from Eqs. (17) and (28)] is not. Such properties become evident in the triangular representation of the solar  $3\nu$  mixing parameter space discussed in [20,32], to which the reader is referred for further details.

Figure 6 shows, in the triangular plot, isolines of  $P_{3\nu}^{\text{QV}}$  (dotted lines) for  $\delta m^2/E$  close to  $1.65 \times 10^{-9}$  eV<sup>2</sup>/MeV, corresponding to about 100 oscillation cycles. More precisely, the six panels correspond to  $\xi = 100 \times 2\pi + \Delta\xi$ , with  $\Delta\xi$  from 0 to  $\pi$  in steps of  $\pi/5$ . The dotted isolines are asymmetric with respect to  $\omega = \frac{\pi}{4}$ , as is the QV correction  $P_{\odot} - c_{\omega}^2$ . For increasing  $s_{\phi}^2$  (upper part of the triangle), the symmetry tends to be restored, mainly because the asymmetric term  $c_{\phi}^4 P_{2\nu}$  in Eq. (17) is suppressed by the prefactor  $c_{\phi}^4$  and, marginally, because

---

<sup>11</sup>In the MSW regime, the mirror asymmetry of the first two octants was explicitly shown in [20].

the effective electron density  $c_\phi^2 N_e$  in  $P_{2\nu}$  is also suppressed.<sup>12</sup> Exact mirror symmetry at any  $\phi$  is restored only if the QV corrections are switched off (solid lines); in such case,  $P_{3\nu}$  is a quadratic form in the coordinates  $s_\phi^2$  and  $s_\omega^2$ , and the isolines are conical curves. In any case,  $P_{ee}$  becomes typically too low (too high) in the central region (in the corners) of the triangle where, as a consequence, one should expect only marginal solutions to the solar neutrino deficit.

The asymmetry with respect to  $\omega = \frac{\pi}{4}$  also shows up in solar neutrino data fits [19]. Figure 7 reports the results of our global (rates + spectrum + day/night) three-flavor analysis in the mass-mixing range  $\delta m^2 \in [10^{-11}, 10^{-8}]$  eV<sup>2</sup> and  $\tan^2 \omega \in [10^{-2}, 10^2]$ , for several representative values of  $\tan^2 \phi$ . We only show 99% C.L. contours<sup>13</sup> ( $N_{\text{DF}} = 3$ ) for the sake of clarity. The theoretical [34] and experimental [35–40] inputs, as well as the  $\chi^2$  statistical analysis [41], are the same as in Ref. [16] (where MSW solutions were studied). Here, however, the range of  $\delta m^2$  is lower, in order to show the smooth transition from the MSW solutions to the QV and finally the JS ones as  $\delta m^2$  is decreased. In particular, the solutions shown in Fig. 7 represent the continuation, at low  $\delta m^2$ , of the LOW MSW solutions shown in Fig. 10 of [16] (panel by panel).<sup>14</sup> As anticipated in the comments to Fig. 6, the mirror asymmetry around  $\tan^2 \omega = 1$  decreases for decreasing  $\delta m^2$  (JS regime); a little asymmetry is still present even at  $\delta m^2 \sim 10^{-10}$  eV<sup>2</sup>, where the gallium rates (sensitive to  $E$  as low as  $\sim 0.2$  MeV) start to feel QV effects. In the region where QV effects are important, the solutions are typically shifted in the second octant ( $\omega \gtrsim \pi/4$ ), since the gallium rate is suppressed too much in the first octant (see also [19]). A similar drift was found for the LOW MSW solution [16]. At any  $\delta m^2$ , the asymmetry decreases at large values of  $\phi$  ( $\tan^2 \phi \gtrsim 1.5$ ) which, however, are excluded by the combination of accelerator and reactor data [21], unless the second mass square difference  $m^2$  turns out to be in the lower part of the sensitivity range of the CHOOZ experiment [42] ( $m^2 \sim 10^{-3}$  eV<sup>2</sup>). For  $\phi = 0$ , the standard two-flavor case is recovered, and the results are comparable to those found in [15]. The Super-Kamiokande spectrum plays only a marginal role in generating the mirror asymmetry of the solutions in Fig. 7, since the modulation of QV effects in the energy domain is much weaker than the one generated by the oscillation phase  $\xi$ . We find that, at any given  $\delta m^2 \lesssim 10^{-8}$  eV<sup>2</sup>,

---

<sup>12</sup>When the effective electron density  $c_\phi^2 N_e$  is small ( $s_\phi^2 \rightarrow 1$ ), the statement that the quasi-vacuum probability  $P_{2\nu}$  does not depend on the production point in the core (see Sec. IV) is not strictly valid, and one should in principle consider also the  $\nu$  source profile. However, since  $P_{2\nu}$  is correspondingly suppressed by  $c_\phi^4$ , the source smearing effect is numerically small, and one can effectively discard it (e.g., by taking the production point at  $r = 0$  at any  $s_\phi^2$ ).

<sup>13</sup>At 95% C.L. the solutions would be mostly located at  $\delta m^2 \lesssim 10^{-9}$  eV<sup>2</sup>.

<sup>14</sup>A technical remark is in order. The minimum value of  $\chi^2$  in the plane of Fig. 7 ( $\chi_{\text{min}}^2 = 31.8$ ) is reached at  $(\delta m^2/\text{eV}^2, \tan^2 \omega, \tan^2 \phi) = (4.4 \times 10^{-10}, 2.4, 0.1)$ . For  $\delta m^2 > 10^{-8}$  eV<sup>2</sup> (MSW regime), the minimum value is  $\chi_{\text{min}}^2 = 27.0$  [16] for the same input data. In order to match the results of Fig. 7 in this work and of Fig. 10 in [16], we have adopted the *absolute* minimum ( $\chi_{\text{min}} = 27.0$ ) to draw the  $\Delta\chi^2 = 11.34$  contours in Fig. 7.

the  $\chi^2$  difference at symmetric  $\omega$  values is less than  $\sim 1$  for the 18-bin spectrum data fit. Therefore, QV effects are mainly probed by total neutrino rates at present.

We think it is not particularly useful to discuss more detailed features of the current QV solutions, such as combinations of spectral data or rates only, fits with variations of *hep* neutrino flux, etc. (which were instead given in [16] for MSW solutions). In fact, while the shapes of current MSW solutions are rather well-defined, those of JS or QV solutions are still very sensitive to small changes in the theoretical or experimental input. Therefore, a detailed analysis of the “fine structure” of the QV solutions in Fig. 7 seems unwarranted at present.

Finally, in Fig. 8 we show sections of the allowed  $3\nu$  solutions (at 99% C.L.) in the triangle representation, for six selected (increasing) values of  $\delta m^2$ . Solutions are absent or shrunk at  $s_\phi^2 \sim 0.5$ , where the theoretical  $\nu$  flux underestimates the gallium and water-Cherenkov data. The lowest value of  $\delta m^2$  ( $0.66 \times 10^{-10}$  eV<sup>2</sup>) falls in the JS regime, so that the ring-like allowed region (which resembles the curves of iso- $P_{ee}$  in Fig. 6) is symmetric with respect to the vertical axis at  $\omega = \pi/4$ . However, as  $\delta m^2$  increases and QV effects become operative, the solutions become more and more asymmetric, and shifted towards the second octant of  $\omega$  [17,19].

Figures 7 and 8 in this work, as well as Fig. 10 in [16], show that solar neutrino data, by themselves, put only a weak upper bound on the mixing angle  $\phi$ . Much tighter constraints are set by reactor data [42], unless the second mass square difference  $m^2$  happens to be  $\lesssim 10^{-3}$  eV<sup>2</sup> (which seems an unlikely possibility). In any case, QV effects are operative also for a small (or zero) value of  $s_\phi^2$ .

## IX. CONCLUSIONS

We have presented a thorough analysis of solar neutrino oscillations in the “quasi-vacuum” oscillation regime, intermediate between the familiar just-so and MSW regimes. The QV regime is increasingly affected by matter effects for increasing values of  $\delta m^2$ . We have calculated such effects both in the Sun and in the Earth, and discussed the accuracy of various possible approximations. We have implemented the QV oscillation probability in a full three-flavor analysis of solar neutrino data, obtaining solutions which smoothly join (at  $\delta m^2 \sim 10^{-8}$  eV<sup>2</sup>) the LOW MSW regions found in [16] for the same input data. The asymmetry of QV effects makes such solutions different for  $\omega < \frac{\pi}{4}$  and  $\omega > \frac{\pi}{4}$ , the two cases being symmetrized only in the just-so oscillation limit of small  $\delta m^2$ .

## ACKNOWLEDGMENTS

We thank J.N. Bahcall for providing us with updated standard solar model results.

## REFERENCES

- [1] J.N. Bahcall, *Neutrino Astrophysics* (Cambridge University Press, Cambridge, England, 1989).
- [2] B. Pontecorvo, Zh. Eksp. Teor. Fiz. **53**, 1717 (1967) [Sov. Phys. JETP **26**, 984 (1968)]; Z. Maki, M. Nakagawa, and S. Sakata, Prog. Theor. Phys. **28**, 675 (1962).
- [3] L. Wolfenstein, Phys. Rev. D **17**, 2369 (1978); S.P. Mikheyev and A.Yu. Smirnov, Yad. Fiz. **42**, 1441 (1985) [Sov. J. Nucl. Phys. **42**, 913 (1985)]; Nuovo Cim. C **9** (1986), 17.
- [4] G.L. Fogli, E. Lisi, and D. Montanino, Astropart. Phys. **9**, 119 (1998).
- [5] S.L. Glashow and L.M. Krauss, Phys. Lett. B **190**, 199 (1987); V. Barger, K. Whisnant, and R.J.N. Phillips, Phys. Rev. D **24**, 538 (1981).
- [6] L. Krauss and F. Wilczek, Phys. Rev. Lett. **55**, 122 (1985).
- [7] See A.S. Dighe, Q.Y. Liu, and A.Yu. Smirnov, hep-ph/9903329, and references therein.
- [8] S. Toshev, Phys. Lett. B **196**, 170 (1987).
- [9] T. Kaneko, Prog. Theor. Phys. **78**, 532 (1987), M. Ito, T. Kaneko and M. Nakagawa, *ibidem* **79**, 13 (1988).
- [10] S.T. Petcov, Phys. Lett. B **200**, 373 (1988); *ibidem* **214**, 139 (1988); *ibidem* **406**, 355 (1997).
- [11] S.T. Petcov and J. Rich, Phys. Lett. B **224**, 426 (1989).
- [12] J. Pantaleone, Phys. Lett. B **251**, 618 (1990).
- [13] S. Pakvasa and J. Pantaleone, Phys. Rev. Lett. **65**, 2479 (1990); J. Pantaleone, Phys. Rev. D **43**, 2436 (1991).
- [14] A.B. Balantekin and J.F. Beacom, Phys. Rev. D **59**, 6323 (1996).
- [15] J.N. Bahcall, P.I. Krastev, and A.Yu. Smirnov, Phys. Lett. B **477**, 401 (2000); C. Giunti, M.C. Gonzalez-Garcia, and C. Peña-Garay, hep-ph/0001101.
- [16] G.L. Fogli, E. Lisi, D. Montanino, and A. Palazzo, hep-ph/9912231, to appear in Phys. Rev. D.
- [17] A. de Gouvêa, A. Friedland, and H. Murayama, hep-ph/0002064.
- [18] A. de Gouvêa, A. Friedland, and H. Murayama, Phys. Rev. D **60**, 093011 (1999).
- [19] A. Friedland, hep-ph/0002063.
- [20] G.L. Fogli, E. Lisi, and D. Montanino, Phys. Rev. D **54**, 2048 (1996).
- [21] G.L. Fogli, E. Lisi, A. Marrone, and G. Scioscia, Phys. Rev. D **59**, 033001 (1999); G.L. Fogli, E. Lisi, D. Montanino, and G. Scioscia, Phys. Rev. D **55**, 4385 (1997).
- [22] S.J. Parke, Phys. Rev. Lett. **57**, 1275 (1986).
- [23] J.N. Bahcall homepage, <http://www.sns.ias.edu/~jnb> (Neutrino Software and Data).
- [24] S.P. Mikheyev and A.Yu. Smirnov, Zh. Eksp. Teor. Fiz. **91**, 7 (1986) [Sov. Phys. JETP **64**, 4 (1986)].
- [25] E. Lisi and D. Montanino, Phys. Rev. D **56**, 1792 (1997).
- [26] A. M. Dziewonski and D. L. Anderson, Phys. Earth Planet. Inter. **25**, 297 (1981).
- [27] M. Narayan and S. Uma Sankar, hep-ph/0004204.
- [28] A. de Gouvêa, A. Friedland, and H. Murayama, hep-ph/9910286.
- [29] S.T. Petcov, Phys. Lett. B **434**, 321 (1998); E.K. Akhmedov, Nucl. Phys. B **538**, 25 (1999).
- [30] J.N. Bahcall and S.C. Frautschi, Phys. Lett. **29B**, 623 (1969).
- [31] J.N. Bahcall, Phys. Rev. D **49**, 3923 (1994).

- [32] B. Faïd, G.L. Fogli, E. Lisi, and D. Montanino, *Phys. Rev. D* **55**, 1353 (1997).
- [33] G.L. Fogli, E. Lisi, D. Montanino, and A. Palazzo, *Phys. Rev. D* **61**, 073009 (2000).
- [34] J. N. Bahcall, S. Basu and M. Pinsonneault, *Phys. Lett. B* **433**, 1 (1998); see also [23].
- [35] Homestake Collaboration, B. T. Cleveland, T. J. Daily, R. Davis Jr., J. R. Distel, K. Lande, C. K. Lee, P. S. Wildenhain, and J. Ullman, *Astrophys. J.* **496**, 505 (1998).
- [36] GALLEX Collaboration, W. Hampel *et al.*, *Phys. Lett. B* **447**, 127 (1999).
- [37] SAGE Collaboration, J. N. Abdurashitov *et al.*, *Phys. Rev. C* **60**, 055801 (1999).
- [38] Kamiokande Collaboration, Y. Fukuda *et al.*, *Phys. Rev. Lett.* **77**, 1683 (1996).
- [39] Y. Totsuka, in *PANIC'99*, XVth Particles And Nuclei International Conference (Uppsala, Sweden, 1999), to appear; Report available at <http://www-sk.icrr.u-tokyo.ac.jp/doc/sk/pub>
- [40] Y. Suzuki for the Super-Kamiokande Collaboration, in *Lepton-Photon '99*, Proceedings of the XIX International Symposium on Photon and Lepton Interactions at High Energies (Stanford, California, U.S.A., 1999), to appear; transparencies available at <http://lp99.slac.stanford.edu>
- [41] G.L. Fogli and E. Lisi, *Astropart. Phys.* **3**, 185 (1995).
- [42] CHOOZ Collaboration, M. Apollonio *et al.*, *Phys. Lett. B* **466**, 415 (1999).

## FIGURES

FIG. 1. Radial profile of the electron density in the Sun from the standard solar model (solid line), together with its exponential approximation (dashed line).

FIG. 2. Isolines of the solar correction term  $P_{\odot} - c_{\omega}^2$  in the mass-mixing plane (solid curves), for standard solar model density [23]. Isolines of MSW resonance radii (dashed curves) are also shown.

FIG. 3. As in Fig. 2, but for the exponential density profile. Dotted and solid lines correspond to analytical calculations and to their semianalytical approximation, respectively.

FIG. 4. Isolines of the Earth correction term  $P_{\oplus} - c_{\omega}^2$  in the mass-mixing plane, for PREM [26] density. The solid and dotted lines correspond to a nadir angle equal to  $0^{\circ}$  and  $45^{\circ}$ , respectively.

FIG. 5. Damping factor for the oscillating term, due to the finite Be line width. See the text for details.

FIG. 6. Three-flavor oscillations: Isolines of  $P_{ee}$  in the triangular representation of the solar  $\nu$  mixing parameter space, for representative values of the oscillation phase  $\xi$ . The dotted and solid lines refer, respectively, to calculations with and without quasi-vacuum effects. When such effects are included, the mirror symmetry  $\omega \rightarrow \frac{\pi}{2} - \omega$  is broken.

FIG. 7. Three-flavor oscillations: Contours at 99% C.L., as derived from a global analysis of neutrino data for  $\delta m^2 \leq 10^{-8}$  eV<sup>2</sup> (quasi-vacuum regime). The asymmetry of the solutions is evident for increasing values of  $\delta m^2$ . The solutions represent the continuation (at low  $\delta m^2$ ) of the MSW 99% C.L. regions reported in Fig. 10 of [16].

FIG. 8. Sections of the  $3\nu$  allowed volume (99% C.L.) for six representative values of  $\delta m^2$  (0.66, 2.36, 6.42, 8.76, 10.8, and  $29.5 \times 10^{-10}$  eV<sup>2</sup>), shown in the solar triangle plot.

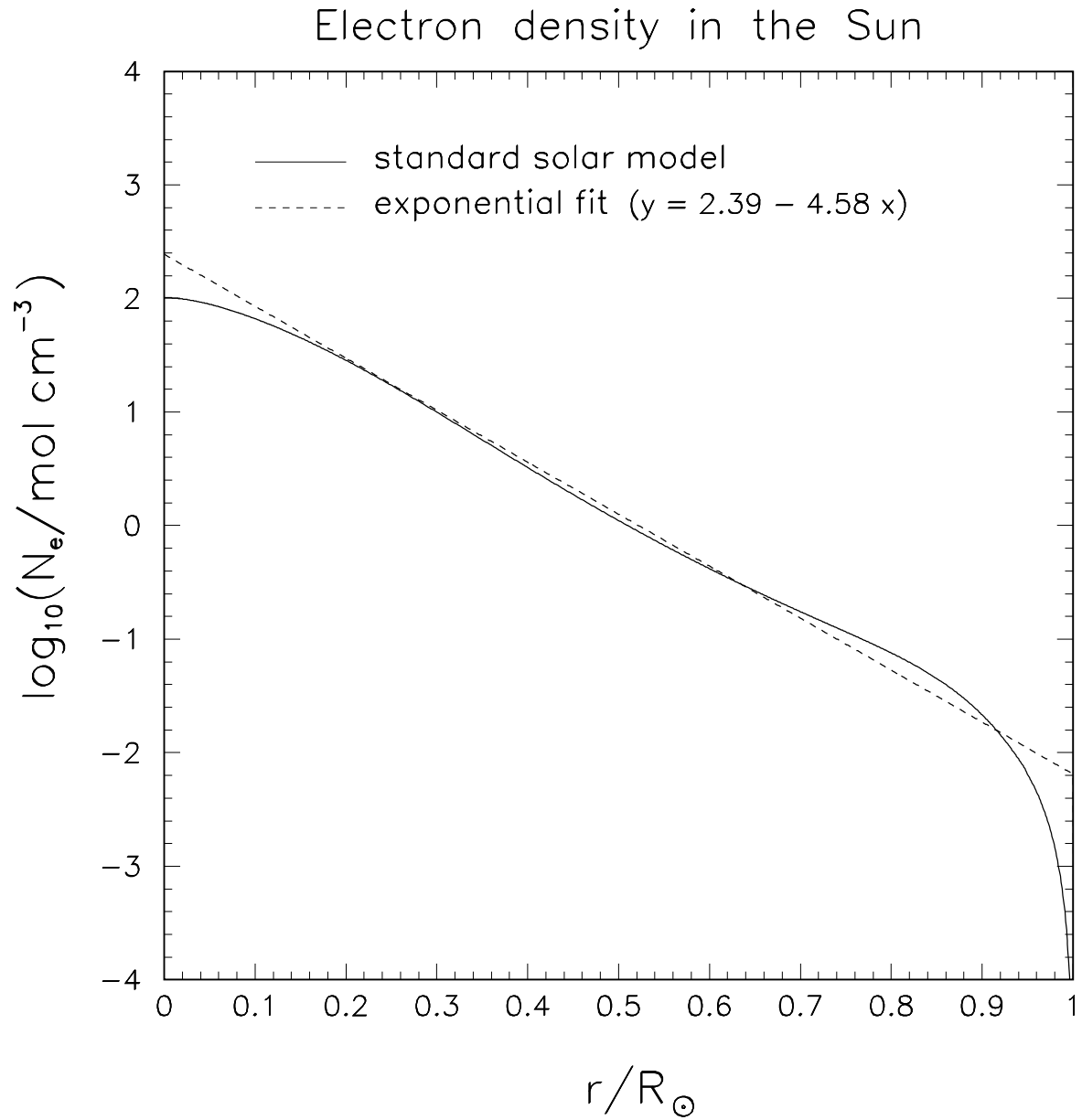


FIG. 1. Radial profile of the electron density in the Sun from the standard solar model (solid line), together with its exponential approximation (dashed line).

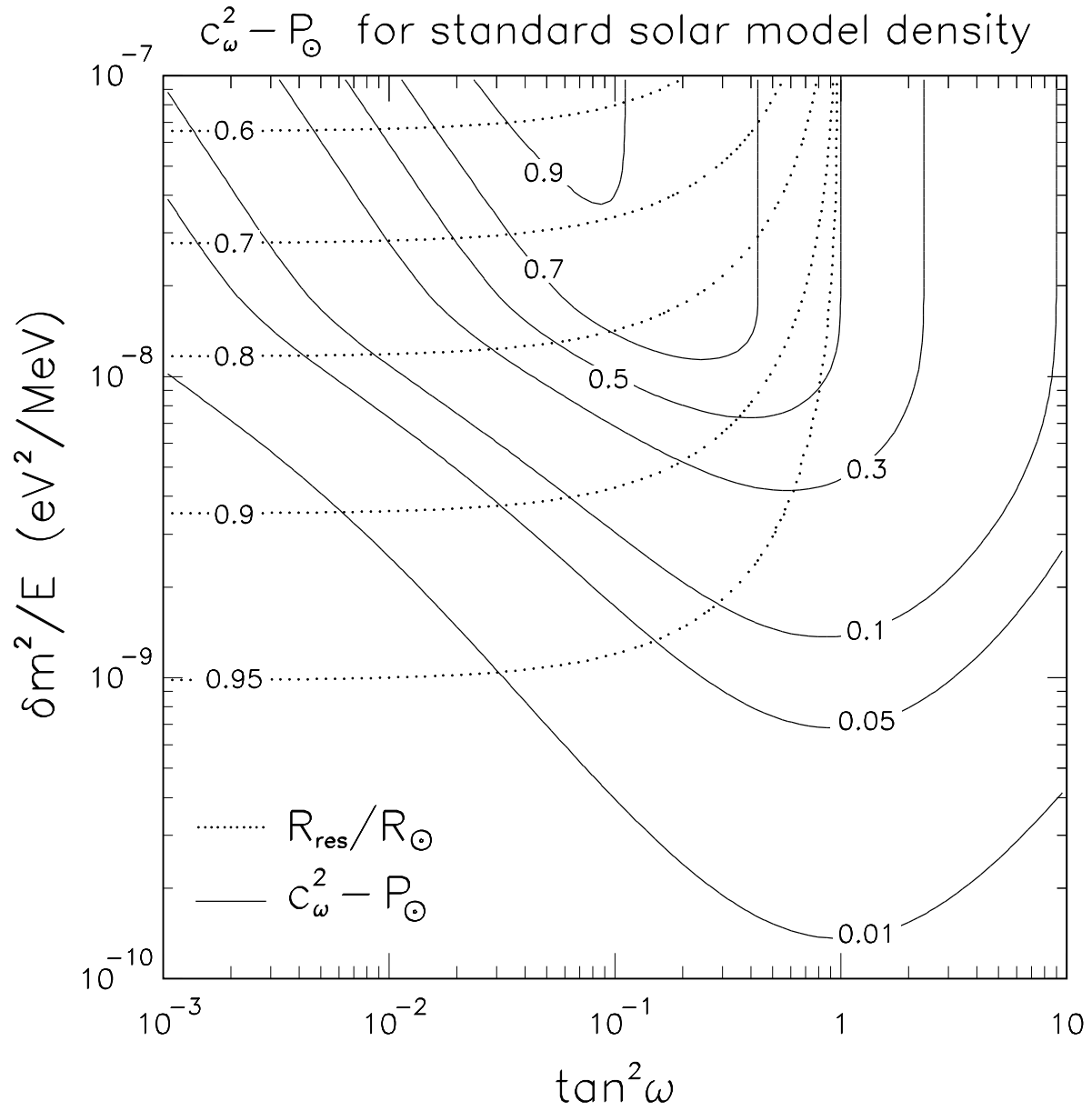


FIG. 2. Isolines of the solar correction term  $P_\odot - c_\omega^2$  in the mass-mixing plane (solid curves), for standard solar model density [23]. Isolines of MSW resonance radii (dashed curves) are also shown.

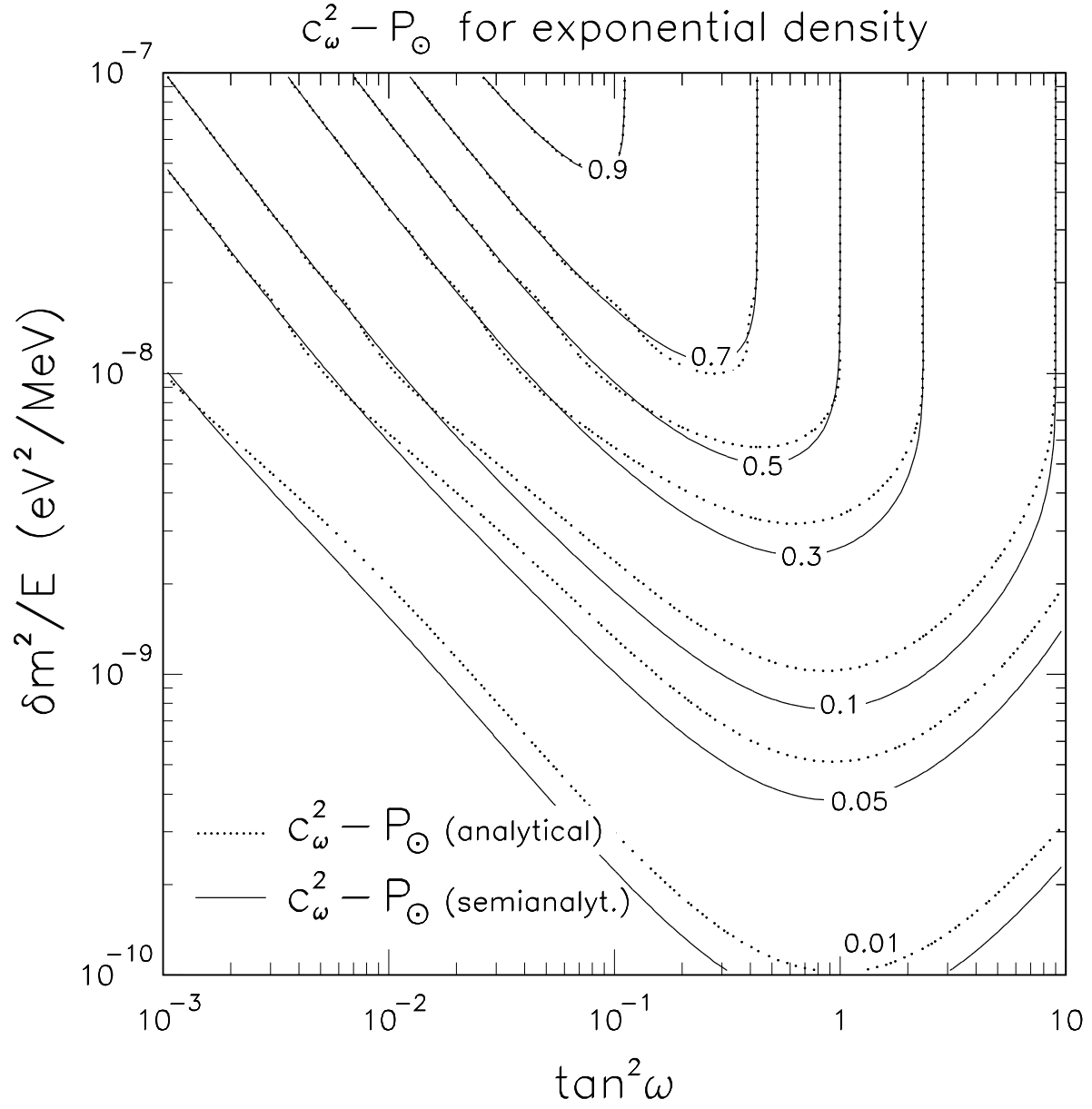


FIG. 3. As in Fig. 2, but for the exponential density profile. Dotted and solid lines correspond to analytical calculations and to their semianalytical approximation, respectively.

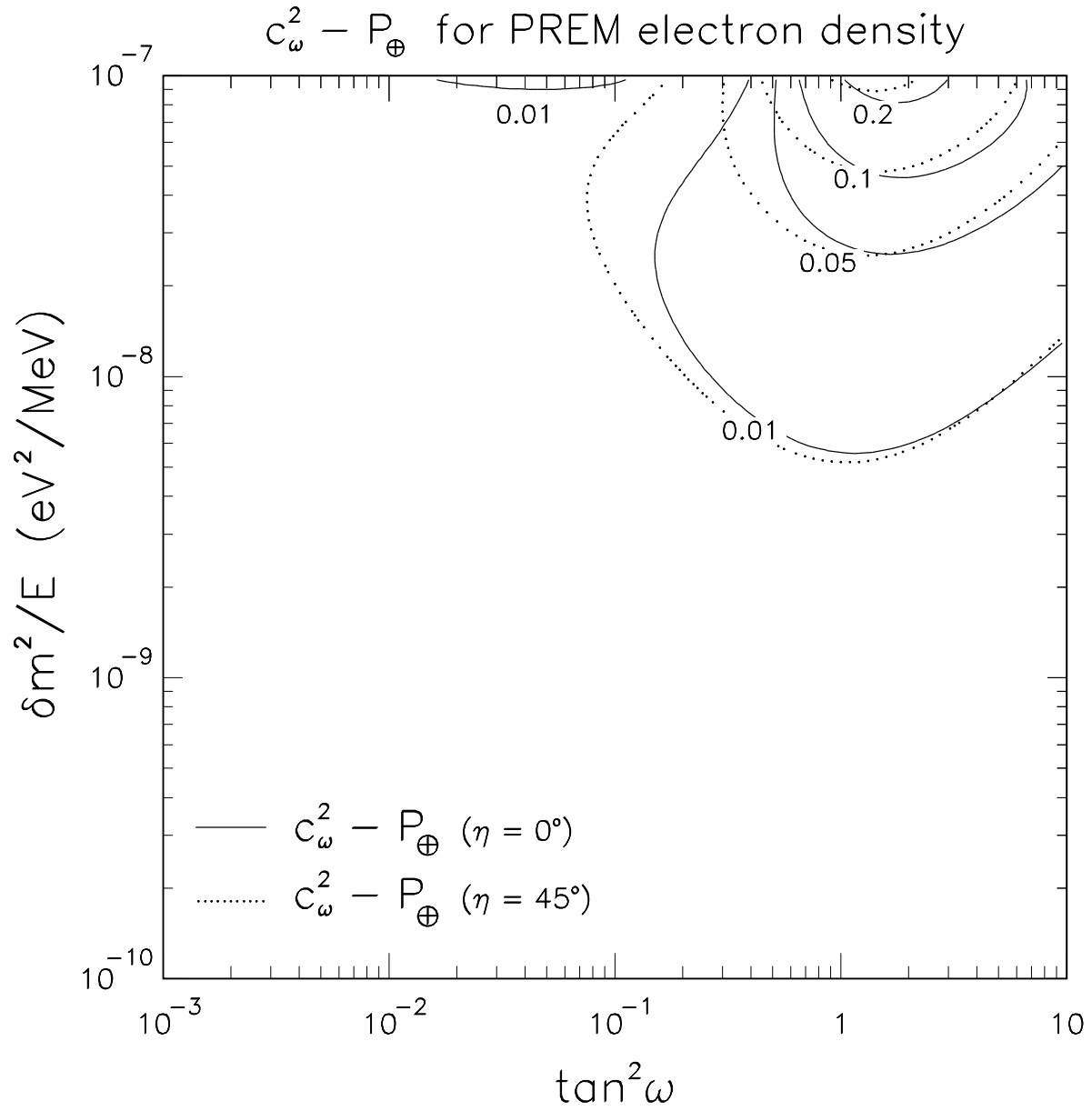


FIG. 4. Isolines of the Earth correction term  $P_\oplus - c_\omega^2$  in the mass-mixing plane, for PREM [26] density. The solid and dotted lines correspond to a nadir angle equal to  $0^\circ$  and  $45^\circ$ , respectively.

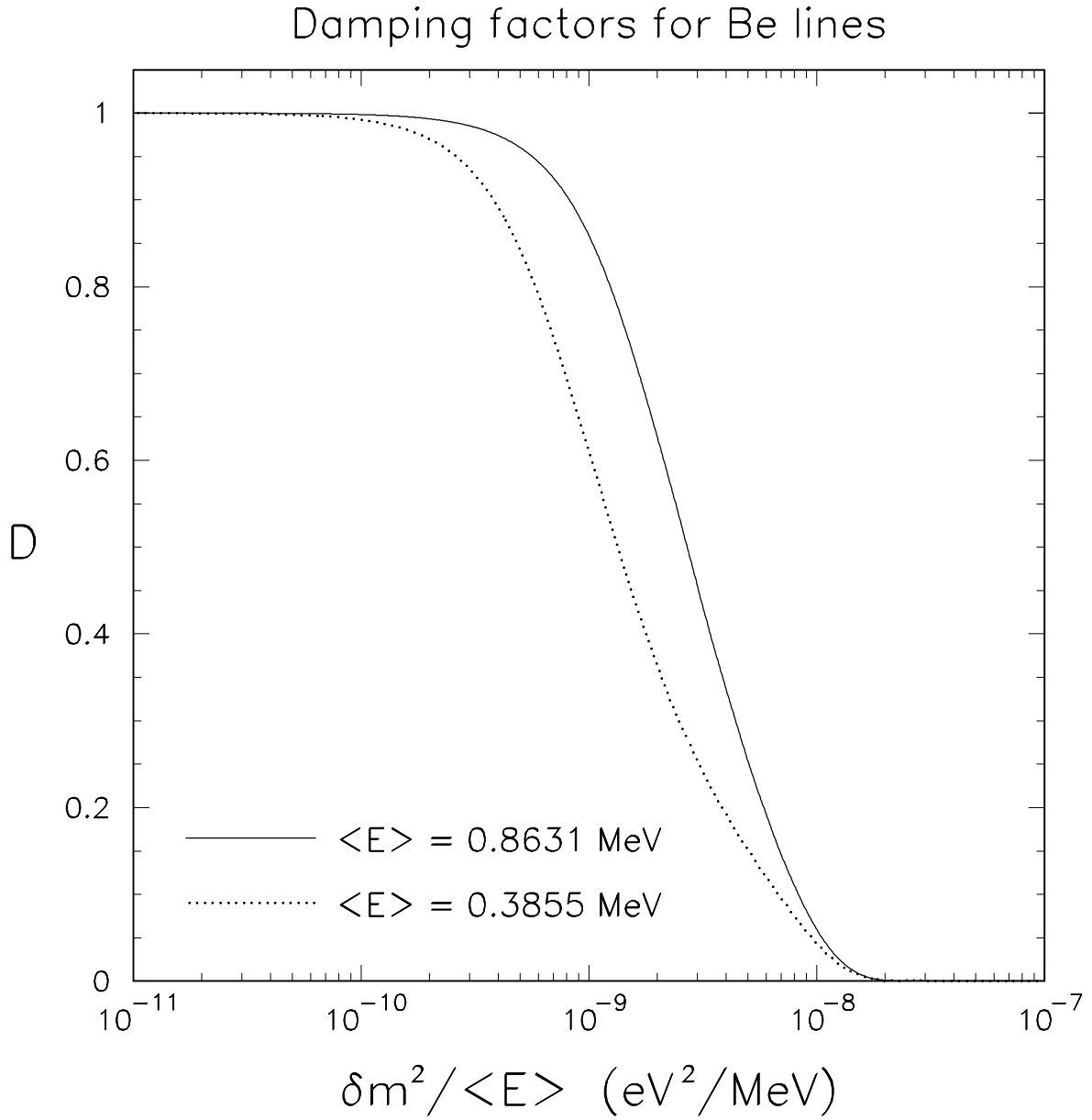


FIG. 5. Damping factor for the oscillating term, due to the finite Be line width. See the text for details.

$3\nu$  mixing: curves of iso- $P(\nu_e \rightarrow \nu_e)$   
for oscillation phase =  $100 \cdot 2\pi + \Delta\xi$

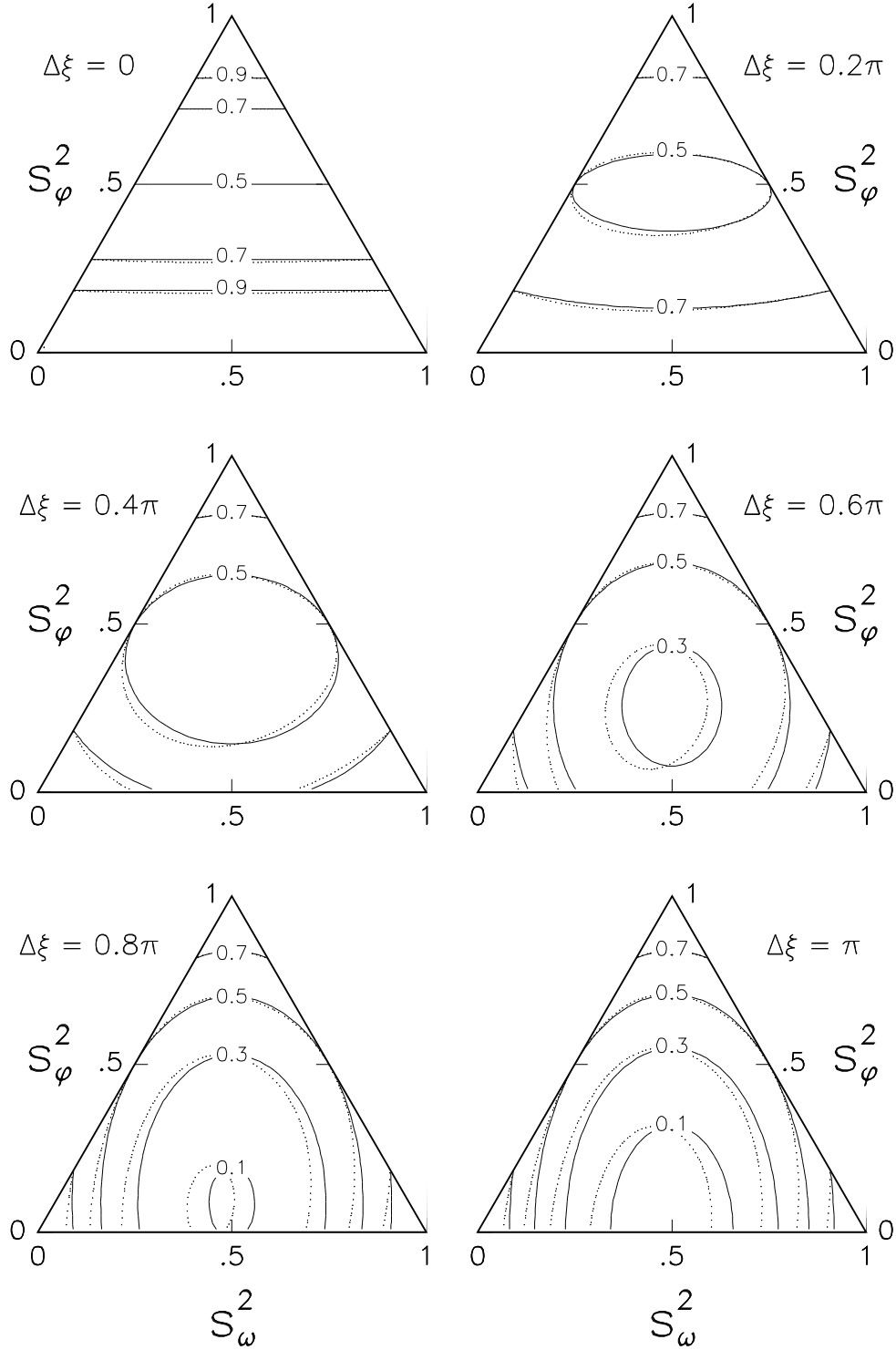


FIG. 6. Three-flavor oscillations: Isolines of  $P_{ee}$  in the triangular representation of the solar  $\nu$  mixing parameter space, for representative values of the oscillation phase  $\xi$ . The dotted and solid lines refer, respectively, to calculations with and without quasi-vacuum effects. When such effects are included, the mirror symmetry  $\omega \rightarrow \frac{\pi}{2} - \omega$  is broken.

### $3\nu$ analysis: Rates + Spectrum + D/N

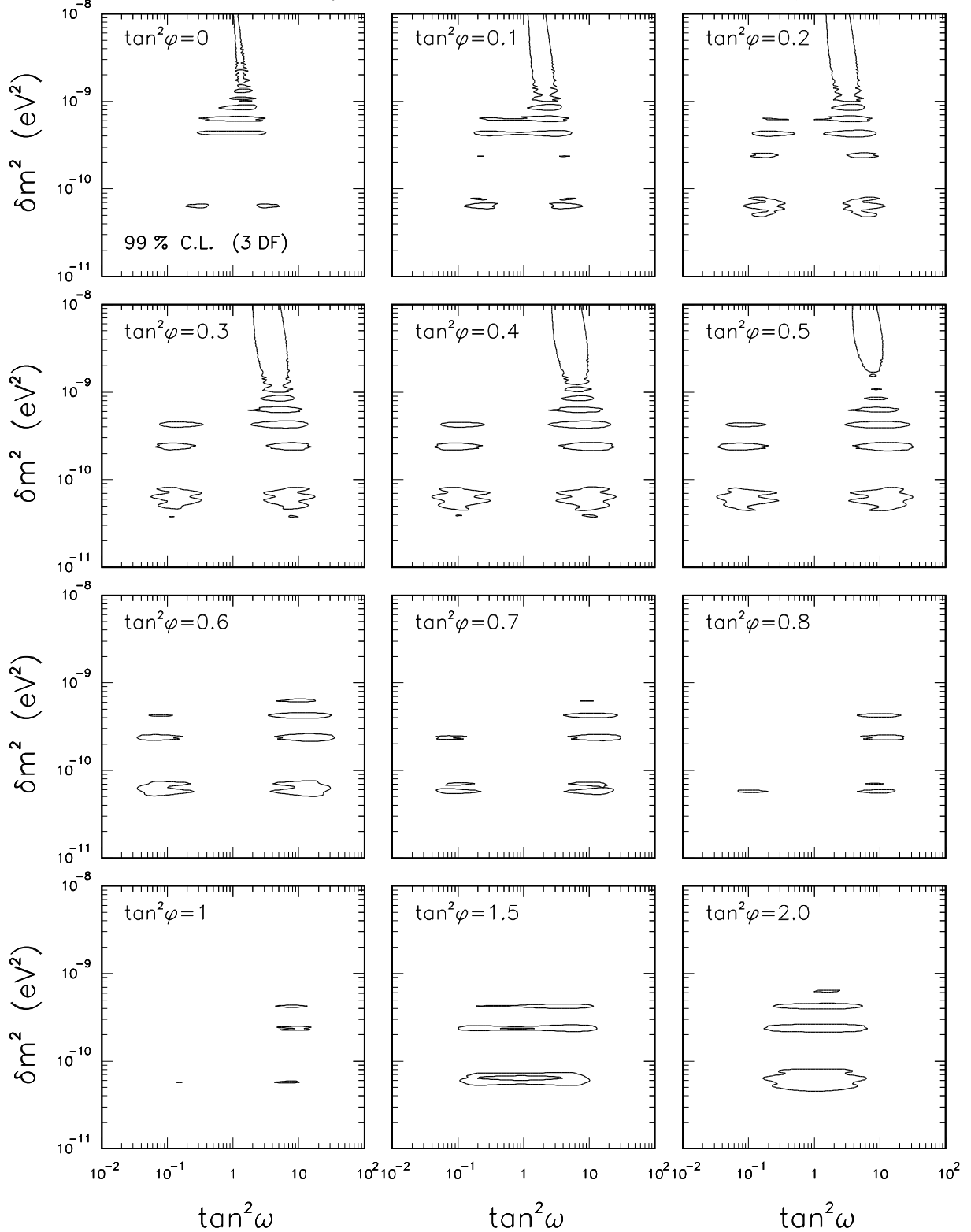


FIG. 7. Three-flavor oscillations: Contours at 99% C.L., as derived from a global analysis of neutrino data for  $\delta m^2 \leq 10^{-8} \text{ eV}^2$  (quasi-vacuum regime). The asymmetry of the solutions is evident for increasing values of  $\delta m^2$ . The solutions represent the continuation (at low  $\delta m^2$ ) of the MSW 99% C.L. regions reported in Fig. 10 of [16].

Solar  $3\nu$  analysis (99 % C.L.)

$$\delta m^2 / 10^{-10} \text{ eV}^2 =$$

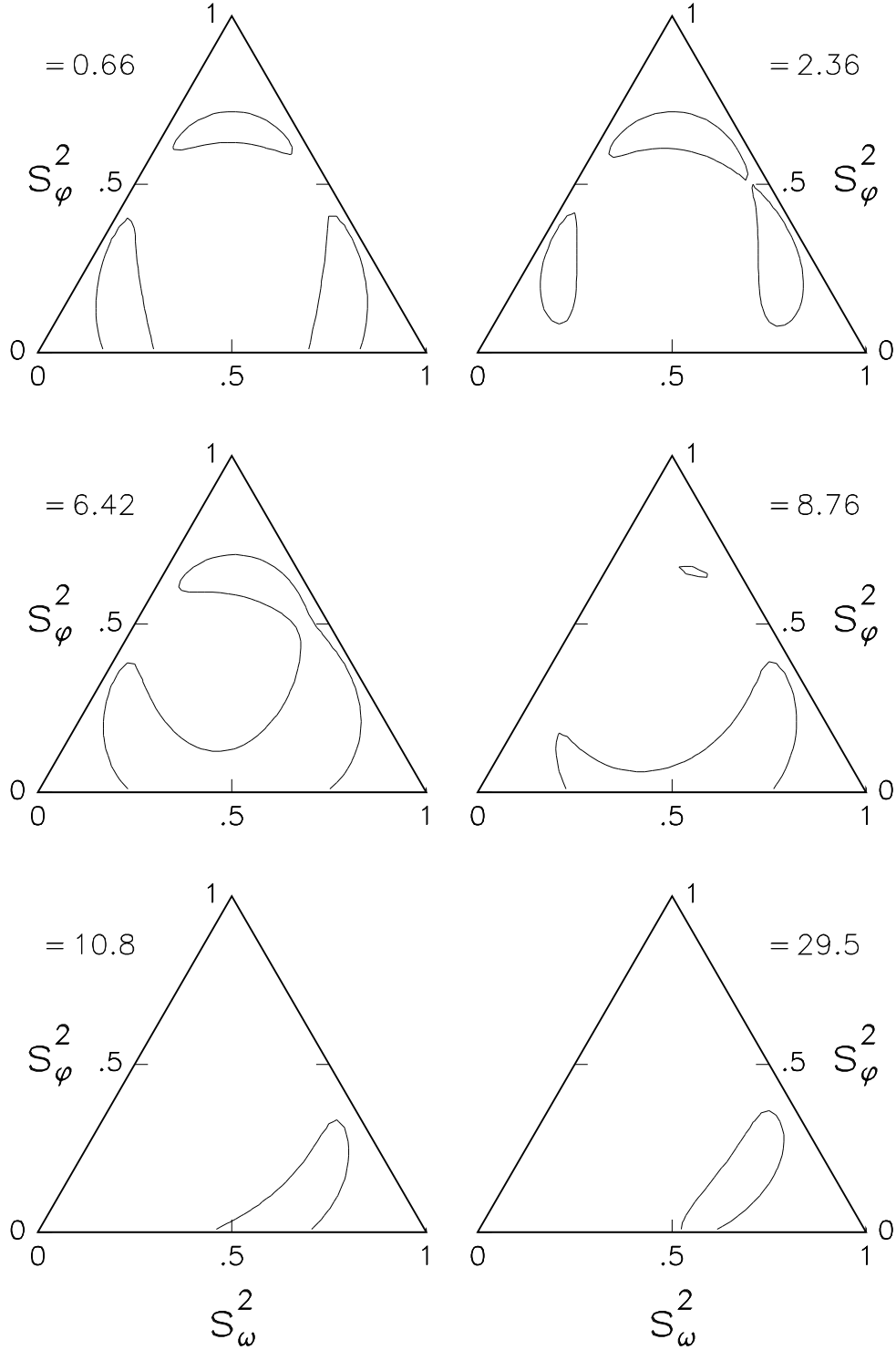


FIG. 8. Sections of the  $3\nu$  allowed volume (99% C.L.) for six representative values of  $\delta m^2$  (0.66, 2.36, 6.42, 8.76, 10.8, and  $29.5 \times 10^{-10} \text{ eV}^2$ ), shown in the solar triangle plot.